

The area-to-mass ratio and fractal dimension of marine flocs



D.G. Bowers^{a,*}, D. McKee^b, C.F. Jago^a, W.A.M. Nimmo-Smith^c

^a School of Ocean Sciences, Bangor University, Menai Bridge, Anglesey LL59 5AB, UK

^b Department of Physics, University of Strathclyde, 107 Rottenrow East, Glasgow G4 0NG, UK

^c School of Marine Science and Engineering, Plymouth University, Drake Circus, Plymouth PL4 8AA, UK

ARTICLE INFO

Article history:

Received 7 October 2016

Received in revised form

10 March 2017

Accepted 14 March 2017

Available online 18 March 2017

ABSTRACT

Optical instruments have proved invaluable in the study of suspended matter in the sea but the measurements they provide are more closely related to the cross-sectional area of the particles in suspension than the mass measured by filtration or predicted by theory. In this paper, we examine the factors controlling the relationship between particle area and mass, using the fractal model of particle structure as a theoretical framework. Both theory and observation agree that the area-to-mass ratio of particles (symbol A^*) decreases with increasing fractal dimension (symbol N_f) as particles hide behind each other in compact flocs. The equation $A^* = 0.253 - 0.081N_f$, in which A^* is in $\text{m}^2 \text{g}^{-1}$ explains 81% of the variance in the area:mass ratio at 151 stations in coastal waters. In contrast, the effect of floc size on A^* is small. Three optical parameters – beam attenuation, diffuse attenuation and remote sensing reflectance, expressed per unit mass of suspended material, all decrease with increasing N_f . As our understanding of the flocculation process grows and it becomes possible to predict the fractal dimension of particles as a function of the environmental conditions in which the flocs form, these results will lead to improved calibration of optical instruments in terms of the mass concentration of suspended materials and to better models of sediment suspension and transport.

© 2017 The Authors. Published by Elsevier Ltd. This is an open access article under the CC BY license (<http://creativecommons.org/licenses/by/4.0/>).

1. Introduction

The tendency for small particles to stick together to form aggregates or flocs is a strikingly widespread phenomenon. The process is observed in the atmosphere, when ice crystals form snowflakes (Stein et al., 2015), in the sea with marine flocs (Eisma et al., 1990; Markussen et al., 2016) and in the dust tails of comets (Schulz et al., 2015); no doubt there are many other examples. The flocculation of marine particles, the subject of this paper, is important because it increases their sinking speed and so helps to improve the clarity of the surface waters of the ocean; the flocculation process will also have a direct effect on the optical properties of the suspended material in a way that, at the moment, is not properly understood. In fact, particle flocculation, and the structures it creates, is currently one of the most fascinating and challenging problems in marine science.

It has been suggested that the way that particles combine to form flocs is not entirely random but that it obeys the mathematical laws of fractals; that is, each floc is composed of self-similar

structures (Krone, 1963; Kranenburg, 1994). In the fractal model, the number N of solid particles in a floc increases with floc size D according to the rule $N = (D/D_0)^{N_f}$ where D_0 is the size of the primary, floc-building, particles and N_f is the fractal dimension (which can lie in the range 1–3). Flocs with a high fractal dimension close to 3 are compact, dense and opaque structures; flocs with low fractal dimension close to 1 are tenuous and stringy (Kranenburg, 1994). In all marine flocs, except for coagulated particles with $N_f = 3$, the space between solid particles is occupied by water; for this reason the density of the flocs is generally less than that of the solid material of the primary particles. The observational evidence that suspended marine flocs are in fact fractals is limited, and mostly circumstantial. However, fractal theory is consistent with an important observed property of marine flocs: their density tends to decrease steadily as their size increases (Hill et al., 1998; Mikkelsen and Pejrup, 2001). This behaviour could not be explained if marine flocs were regular structures of particles separated by a fixed distance (in which case the density tends to a constant value at large sizes). For a fractal structure, the mass is proportional to the number of solid primary particles, N , and the volume (we shall assume) is proportional to D^3 and so the density scales as D^{N_f}/D^3 or $D^{N_f - 3}$. For particles with a fractal dimension less than 3, the

* Corresponding author.

E-mail address: d.g.bowers@bangor.ac.uk (D.G. Bowers).

density will therefore decrease with size. The fractal dimension of small marine flocs is difficult to measure directly. Estimates of fractal dimension can be made by photographing flocs (Chen and Eisma, 1995; Kilps et al., 1993) and by inference from settling speeds (Dyer and Manning, 1995) and by plotting density against size. Alternatively, if a fractal structure is assumed, N_f can be calculated by matching the calculated and observed mass of the floc (Braithwaite et al., 2010).

The area-to-mass ratio of a particle is an important quantity when considering the interaction between suspended matter and light. Optical instruments used to measure the concentration of material in suspension in seawater, including beam transmissometers, turbidity meters and radiometers (both in-water and on a remote sensing platform such as a satellite) are sensitive to the cross-sectional area of the particles (Baker and Lavelle, 1984; Bale et al., 1994; Bowers and Braithwaite, 2012). The calibration of these instruments in terms of the mass concentration, measured on a filter, is therefore sensitive to the particle area:mass ratio. Similarly, numerical models of suspended sediments (Jones et al., 1996; Guillou et al., 2015) invariably predict mass concentration. A quantitative comparison of models to observations made by optical instruments will depend on the area to mass ratio of the particles in the study area. Several studies have reported the excellent correlation between particle area:mass ratio and inherent optical properties, expressed per unit particle mass (Bowers et al., 2009; Neukermans et al., 2012). It is therefore likely that the factors that influence the area to mass ratio will also be important for mass-specific inherent optical properties. Theoretical models of optical properties which incorporate the fractal dimension of the particles have been used successfully to predict mass-specific optical properties (Stavn, 2011).

In the simplest case, the ratio of the area to mass of particles can be calculated from their geometry. For a suspension of identical spheres of diameter D and density ρ , the cross sectional area of the suspension scales as D^2 and the mass as ρD^3 , so the area-to-mass ratio is proportional to $1/(\rho D)$. In fact, for a cloud of particles with any size distribution the area:mass ratio can always be written in terms of $1/(\rho D)$ where ρ and D are defined in a suitable way to represent the average density and size of the particles. For a given mass of particles with constant density, the population cross-sectional area will therefore increase with decreasing size. A familiar example of this phenomenon in the atmosphere is the difference in visibility in rain and mist. The smaller but more numerous mist particles have a greater cross sectional area and are therefore better at scattering light.

The same phenomenon does not happen so readily in the sea, however. For marine flocs whose density varies inversely with particle size, changes in particle size and density tend to cancel each other out in the expression $1/(\rho D)$ and so particle area per unit mass and mass-specific optical properties are relatively insensitive to changes in particle size (Hill et al., 2011). A fortunate consequence of this effect is that the calibration of optical instruments against the mass concentration of suspended flocculating material is often successful over a wide range of particle sizes. However, there remains about an order of magnitude variation in observed mass-specific optical properties, including beam attenuation (Hill et al., 2011; Bowers and Binding, 2006), scattering (Neukermans et al., 2012; Bowers et al., 2009) and backscattering (Neukermans et al., 2012). Hill et al. (2011) discuss the reasons for this remaining variability, including the particle structure and component particle density. Because mineral material is denser than organic material in the sea, floc density and therefore the area to mass ratio will depend on the mineral content of flocs; this effect can be measured (Hill et al., 2013) but produces a change of only about 2 in the area-mass ratio. However the apparent density of a floc (the dry

mass divided by the volume in situ – see appendix) will depend on the way that the particles are packed into the floc, which will be a function of the fractal dimension. Note, incidentally, that there are a number of definitions of marine floc density in the literature. Kranenburg (1994) originally applied the concept of fractals to excess density (floc density minus the density of water; it is this density which is relevant to calculating settling speeds). However, fractal structure applies equally well to apparent density, so long as the density used for the primary particle is also the apparent density. Unless otherwise stated, it is the apparent density that we use in this paper.

The fractal model, coupled with an assumption about the particle size distribution, provides a theoretical framework for calculating the area to mass ratio of marine flocs, as described in the next section. Our first aim of this paper is to test these calculations against observation. A second aim is to examine relationships between mass-specific optical parameters (attenuation and reflection coefficients) and particle structure as represented by the fractal dimension.

2. Theoretical background

Following a convention often used in the study of the optical properties of particles we will denote quantities expressed per unit dry particle mass by an asterisk. So, the total floc cross-sectional area per unit mass of material is expressed as A^* (see Table 1 for notation). We begin with an analysis of the area-to-mass ratio of a suspension of identical fractal particles. In this simple case, an analytical solution for A^* is easily found and it turns out that this solution contains all of the important features of the more general solution (obtained numerically and given in the second part of this section) when the particles have a range of sizes.

Consider, then, a suspension of n identical flocs whose size can be represented by the dimension D . Each floc contains N primary particles, each of size D_0 and density ρ_0 . We will follow the usual convention and assume that the area of each floc is proportional to D^2 and the volume to D^3 , however we note that this may not be correct for low fractal dimension flocs [dealing with the geometry of irregular shaped particles is part of the challenge of this subject. For a stringy floc with N_f close to 1, for example, the area and volume are more likely to both scale with D]. When dealing with irregular shaped flocs it seems overly specific to assume spherical geometry and so we will take the particle area as equal to D^2 and its volume as D^3 . With these provisos, the ratio of the cross sectional area of the floc population to their dry mass (excluding water) is

$$A^* = \frac{nD^2}{nN\rho_0D_0^3} = \frac{D^2}{N\rho_0D_0^3} \quad (1)$$

if the flocs are fractals, the number of primary particles in each floc is $N = (D/D_0)^{N_f}$ where N_f is the fractal dimension. Making this substitution, and re-arranging gives, for the area-to mass ratio of a suspension of identical fractal flocs:

$$A^* = \frac{1}{\rho_0D_0} \left(\frac{D_0}{D}\right)^{N_f-2} \quad (2)$$

from which it can be seen that if N_f is exactly 2, $A^* = 1/(\rho_0D_0)$; the area-to-mass ratio of the flocs becomes independent of their size and just depends on the characteristics of the primary particles. This situation is equivalent to the floc density being exactly proportional to $1/D$: changes in density and size cancel out and the area-to-mass ratio of any size floc is the same. Increasing N_f to 3 makes the area-to-mass ratio equal to $1/(\rho_0D)$; a change in fractal

dimension from 2 to 3 produces a change in A^* by a factor D/D_0 . For flocs with a size scale at least an order of magnitude greater than the component particle size, this factor will be enough to account for the observed variation in mass-specific optical properties.

Fig. 1a shows a graph of A^* against fractal dimension calculated using equation (2). The figure is drawn for values of the primary particle size and density of $4 \mu\text{m}$ and 2000 kg m^{-3} respectively and for three floc sizes, 10, 20 and $30 \mu\text{m}$. The area:mass ratio of the flocs decreases as the fractal dimension increases and the flocs become more compact. As the fractal dimension increases, the primary particles are better able to hide behind each other, reducing the projected area of the floc. It can be seen that the three curves for different sized flocs cross at the same area to mass ratio when $Nf = 2$. For values of fractal dimension in the range 2–3, the area-to-mass ratio decreases as the particle size increases (although the absolute change is small), but for values of Nf less than 2, the value of A^* increases as floc size increases. The increase in the area:mass ratio with increasing floc size is counter-intuitive. The reason for the behaviour seen in Fig. 1a is that the area of the

floc scales as D^2 but the mass of the floc when $Nf < 2$ scales as D to a power less than 2; the area-to-mass ratio therefore increases as the floc size increases. The curves when $Nf < 2$ should therefore be interpreted with caution. When $Nf > 2$, however, it seems reasonable to keep the assumption that particle area scales as D^2 and most of the results described in this paper lie in the range $2 < Nf < 3$.

A more realistic description of the area-to-mass ratio of a suspension can be achieved by adapting the solution to allow for a range of floc sizes. It is commonly observed that the number of particles per unit volume in the ocean decreases with increasing size according to the Junge distribution (Babin et al., 2003):

$$n(D) = n_0 D^{-J} dD \quad (3)$$

where $n(D)$ is the number of particles, per unit volume of water, in the size range $D-D + dD$, n_0 controls the absolute number of particles and J sets the slope of the size distribution. Typically J is observed to lie in the range 3–5 in the ocean (Babin et al., 2003). The cross sectional area, per unit volume, of particles in suspension can be calculated numerically by integration:

$$A = \int_{D1}^{D2} n(D) D^2 dD = n_0 \int_{D1}^{D2} D^{2-J} dD \quad (4)$$

where $D1$ and $D2$ are the size of the smallest and largest particles in the suspension. The mass of the particles per unit volume is given by

$$M = \int_{D1}^{D2} n(D) \rho(D) D^3 dD \quad (5)$$

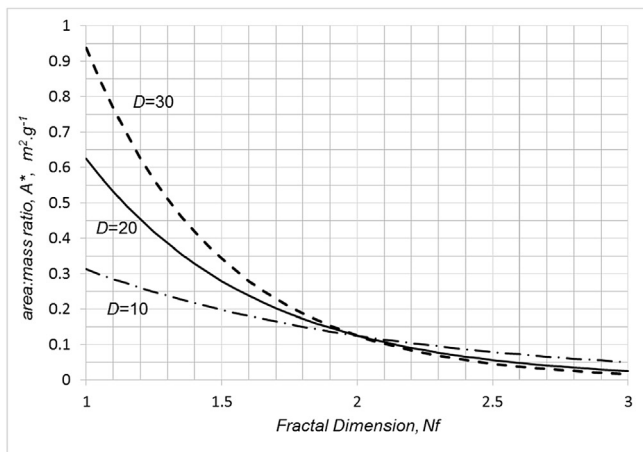
where $\rho(D)$ is the apparent, or effective, density (see appendix) equal to the dry mass of the particles (without the water in the spaces) divided by the volume of the particle in situ. In making this calculation, the apparent density is assumed to change with floc size according to the fractal model, namely:

$$\rho(D) = \rho_0 \left(\frac{D}{D_0} \right)^{Nf-3} \quad D > D_0$$

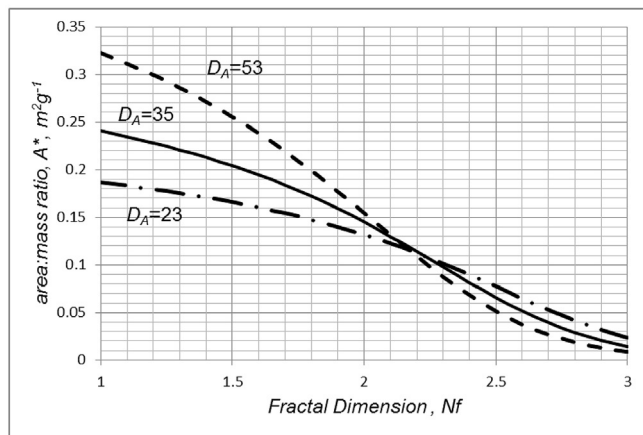
$$\rho = \rho_0 \quad D \leq D_0 \quad (6)$$

Note that the approach we have used here is to allow particles to have a range of sizes between $D1$ and $D2$. Particles whose size is greater than that of the primary particles (D_0) are assumed to be flocs and their density decreases with size according to the fractal model. Particles smaller than the primary particle size are assumed to have a constant density equal to that of the primary particles. Additionally, we have assumed that the fractal dimension is constant independent of the size of the floc, although we note that there is evidence that Nf becomes less as D increases (Khelifa and Hill, 2006).

The area-to-mass ratio of the suspension is obtained by dividing (4) by (5). If the limits of the integrals for area and mass are the same, the ratio when $Nf = 2$ is again $1/(\rho_0 D_0)$ regardless of the value of J . However, to be consistent with the measurements described in the next section, we have chosen different limits for the two integrals. For particle area, which is measured with a LISST 100X type C, the size limits are 2.5 and $500 \mu\text{m}$. For particle mass, which is measured on GF/F filters, the relevant lower size limit is the nominal pore size of the filter, $0.7 \mu\text{m}$. It is rare to see particles larger than 1 mm on a filter: particles larger than this are difficult to maintain in suspension, and so we have taken 1 mm as the upper size limit for calculating particle mass. The results of the numerical



a)



b)

Fig. 1. (a) Theoretical form for the change, with fractal dimension, of the area:mass ratio of a suspension of identical particles. The curves are calculated using equation (2) in the text and primary particle size and density of $4 \mu\text{m}$ and 2000 kg m^{-3} respectively. The curves are drawn for 3 floc sizes of 10, 20 and $30 \mu\text{m}$.

(b) Theoretical form for the change, with fractal dimension, of the area:mass ratio of a suspension of particles with a size distribution given by equation (3). The curves are calculated numerically as described in the text using a primary particle size and density of $4 \mu\text{m}$ and 2000 kg m^{-3} respectively. The curves are drawn for 3 'mean' particle sizes as represented by the Sauter diameter D_A in μm .

solution, unlike the analytical solution, are therefore not general, but have been tuned to match the observational methods.

Fig. 1b shows the area-to-mass ratio of a suspension of particles with a size distribution given by equation (3) and with the primary particle size and density as before, namely $4 \mu\text{m}$ and 2000 kg m^{-3} (we return to the appropriateness of these values in the discussion). The value of the primary particle size and density controls the numerical value of A^* for a given Nf but not the shape of the curve nor the tendency for A^* to decrease with increasing Nf . The solution has been determined for 3 different values of the slope parameter J ; changing the value of J changes the mean size of the particles in suspension. We have represented the mean particle size by the Sauter diameter, the ratio of the total volume to the total cross-sectional area of particles (i.e. $D_A = V/A$). The Sauter diameter just depends on the value of J and the integration limits and it increases as J decreases.

Fig. 1b shows the same general features as Fig. 1a: the area-to-mass ratio of the particles decreases as the fractal dimension increases and the flocs become more compact. There is a crossing point of the three curves which divides a region where A^* increases with particle size from one where it decreases with particle size (the crossing point in this numerical solution occurs at a value of Nf somewhat greater than 2; this shift is caused by the fact that the limits of integration in equations (4) and (5) are different).

An alternative way of presenting the results of the numerical calculations is shown in Fig. 2, in which we have contoured the values of A^* as a function of the slope of the size distribution J and the fractal dimension Nf . The largest values of A^* occur for the big, low fractal dimension flocs in the bottom left of the diagram. The contours between $Nf = 2$ and 3 show that the largest change in A^* is caused by changing Nf ; the mean size of the particles (as represented by J or D_A) is not so important.

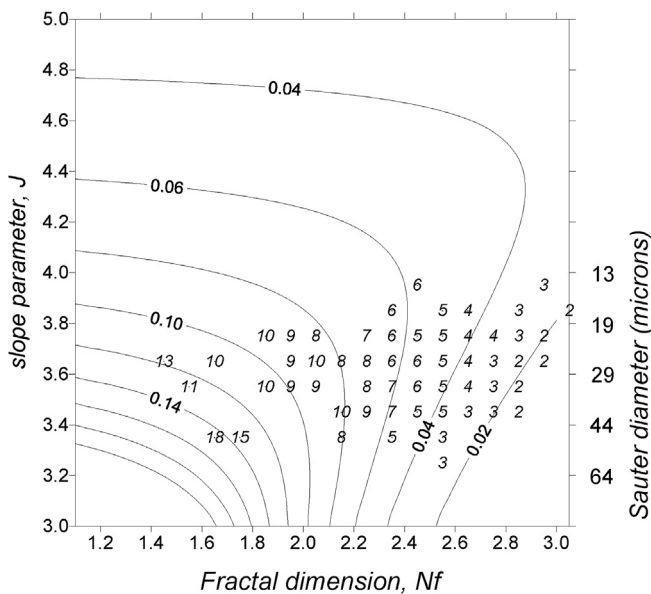


Fig. 2. Contour plot of the area-to-mass ratio A^* (in units of $\text{m}^2 \text{g}^{-1}$) as a function of the slope of the size distribution, J , and the fractal dimension of the flocs Nf . The contour interval is $0.02 \text{ m}^2 \text{g}^{-1}$. The contours have been drawn using the numerical calculations of A^* as described in the text. The super-imposed numbers show observations of A^* (converted to units of $\text{m}^2 \text{g}^{-1}$ times 100 for clarity) averaged into grid elements of 0.1 units of J and Nf . The figures down the right vertical axis show the Sauter diameter, D_A , (in μm) for the corresponding value of J and the size limits of the LISST 100X instrument, namely 2.5 and $500 \mu\text{m}$.

3. Observational methods

Observations of particle cross-sectional area and mass were made on 11 field campaigns and at 151 stations along the south and west coasts of Great Britain over the period June 2008–June 2012 (Fig. 3 and Table 2). The procedure at each station was essentially the same. A LISST 100X type C laser diffraction instrument (Sequoia Scientific Inc.; Agrawal and Pottsmith, 2000) was lowered in a frame from the ship and the depth-averaged volume of particles in 32 size classes in a water column from the surface to a depth of 10 m (or the bottom, if shallower) was measured. The LISST uses measurements of forward scattering to reconstruct the particle size distribution by applying Mie's solution to Maxwell's theories of light scattering by small particles. Spherical particle geometry and constant refractive index are implicit in this reconstruction. There are questions about how the LISST interprets the effect of particles outside its range and how it deals with multiple scattering centres within an aggregated particle (Graham et al., 2012), but for the purposes of this paper we have taken the LISST data at face value. The cross sectional area of particles in suspension A (units m^2 per m^3 of water or m^{-1}) was calculated by summing the area of particles in each size class (that is the area of particles in a size class centred on D_i is calculated as V_i/D_i where V_i is the volume of particles in that size class). The total volume of particles in suspension V (units $\mu\text{l l}^{-1}$) was calculated as the sum of the volumes in the 32 size classes of the LISST.

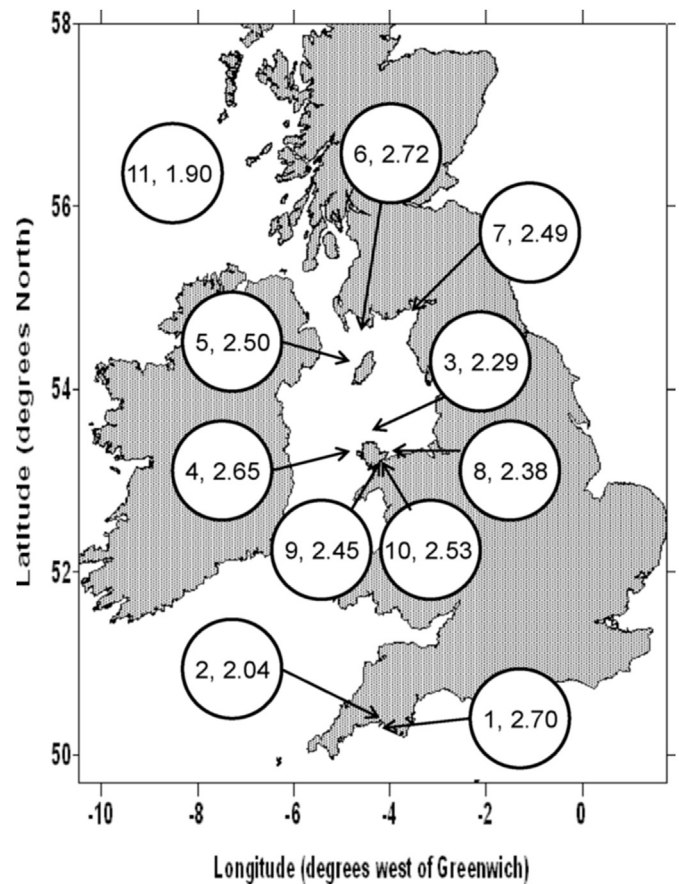


Fig. 3. Shows location of the field campaigns on the south and west coasts of Great Britain. The first figure in each circle refers to the location number given in Table 2 and the second figure in the circle is the estimated mean fractal dimension of the flocs at that location. There is some evidence that higher fractal dimensions are found at high tidal energy sites, such as 4 and 6 and lower fractal dimensions are common at low energy sites, such as 11.

At each station a surface water sample was collected at a depth of 0.5 m, either in a bucket or in a rosette sampler on the CTD and triplicate sub-samples were filtered through Whatman GF/F filters as described in Binding et al. (2005). The filters were subsequently dried and weighed, baked (at 500 °C for 3 h to remove organic material) and weighed again. This procedure gives the mass concentration of total suspended solids (TSS) and mineral suspended solids (MSS) in units of mg l^{-1} or g m^{-3} . The area-to-mass ratio of particles in suspension was calculated by dividing the area of the particles by the mass concentration of total suspended solids. This procedure gives a value in m^2 per gram of particles. Note that the area of the particles is derived from in situ measurements and can be expected to include the water between the solid particles in a floc as well as the solid parts of the floc and free-floating particles outside the floc (Graham et al., 2012). The mass has been measured after removing water. The apparent density of the particles in suspension was calculated as TSS/V and is expressed in kg m^{-3} .

To fit a particle size distribution of the form given by equation (3) to the data, the number, n , of particles in each of the 32 LISST size classes was determined by dividing the total particle volume of particles in that class by the volume of a single particle with a diameter, D , equal to the mean diameter for that class. The slope and intercept of the best fit line to a plot $\ln[n(D)/dD]$ (where \ln is the natural logarithm and dD is the difference between the largest and smallest sizes in each class) against $\ln D$ was then determined by least squares analysis. The absolute value of the slope is the parameter J in equation (3) and the intercept on the y-axis (when $D = 0$) is equal to $\ln(n_0)$. The coefficient of determination, R^2 , for the fit was recorded for each station.

The fractal dimension of the flocs was calculated using an extension of the procedure described in Braithwaite et al. (2010). The mass concentration, M , of the flocs in suspension is calculated from their volume and density, assuming a fractal structure, using equations (5) and (6). The integral in equation (5) is solved numerically, and the number of particles, n , in each size step, is calculated from the Junge distribution (equation (3)) using the value of J and n_0 determined from the fit to the LISST data. To be consistent with the mass measured on the filters, the limits of integration for calculated mass are set to $D1 = 0.7 \mu\text{m}$ to $D2 = 1000 \mu\text{m}$. Braithwaite et al. (2010) used this method to determine the properties of the primary particles as well as the fractal dimension, but here we constrain the solution by choosing the same values of $4 \mu\text{m}$ and 2000kg m^{-3} for the size and density of the primary particles used to construct the theoretical curves. These values lie within the range of values found in the literature (Winterwerp, 1998; Fettweis, 2008; Braithwaite et al., 2010). The mass concentration is calculated using equations (5) and (6) for all values of fractal dimension N_f in the range 1–3 and the fractal dimension which gives the least squared difference between calculated and measured mass concentration (TSS) is noted. As reported in Braithwaite et al. (2010) there is a very sharp minimum when this mass difference is plotted against N_f (an example from two stations in the current dataset is shown in Fig. 4). This very clear minimum appears to lend support, albeit indirect, for the idea that marine flocs can be represented as fractals.

Measurements of beam attenuation, c , were made using the beam transmissometer fixed to the CTD (conductivity-temperature-depth sensor) on the RV Prince Madog. This transmissometer is a Sea Tech T1000 (Sea Tech Inc, Corvallis, Oregon) operating at 660 nm with a 20 cm pathlength. At some stations, vertical profiles of downwelling irradiance and upwelling radiance were made with a PRR (profiling reflectance radiometer; Biospherical Instruments, San Diego California). The diffuse attenuation coefficient for

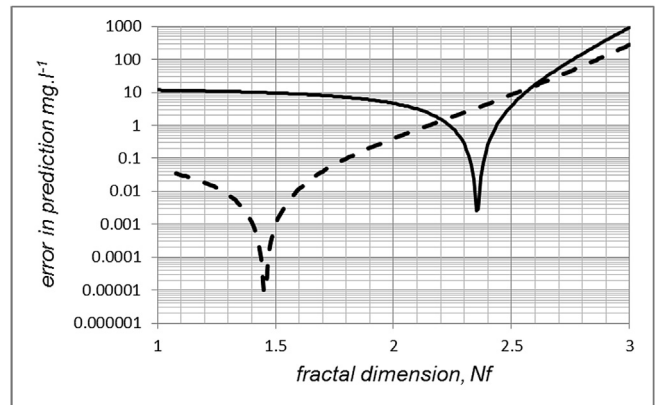


Fig. 4. Illustration for two stations of the fitting technique used to determine the fractal dimension of the particles in suspension. The root-mean-square error between the measured mass concentration TSS and the mass concentration predicted by equation (5) is calculated over the range of fractal dimension $1 < N_f < 3$. The value of N_f which gives the minimum error is chosen. In this figure, the solid curve shows the result for a high tidal energy station in Conwy Bay in July 2009 for which $N_f = 2.35$ and the dashed curve for a low tidal energy station in the western isles of Scotland in June 2012 for which $N_f = 1.42$.

Photosynthetically Active Radiation $K_D(\text{PAR})$ was determined as the slope of a plot of the logarithm of downwelling irradiance (scaled by surface irradiance) down to a maximum depth of 10 m. The reflection coefficient in the red part of spectrum, at 665 nm, is the best single-band reflectance for satellite remote sensing of suspended sediments (Binding et al., 2005; Gohin et al., 2005; Mitchell et al., 2014). The reflectance was calculated by extrapolating downward irradiance and upward radiance at this wavelength to just below the sea surface and taking the ratio to give the radiance, or remote sensing, reflectance (with units of Steradians^{-1}). Further details of these methods used in deploying the optical instruments and in analysing the resulting data can be found in Binding et al. (2005).

4. Results

4.1. The area-to-mass ratio of suspended particles and their fractal dimension

Table 2 summarises the mean values of the parameters measured and calculated on each of the field campaigns and Table 3 summarises the overall mean value and range of the measurements. In Fig. 5, we have plotted the area-to-mass ratio A^* at each station against the calculated fractal dimension and superimposed the theory lines from Fig. 2b. The values of A^* have also been averaged into grid elements of 0.1 units of J and 0.1 units of N_f and plotted on the contours of Fig. 2.

The observations generally support the idea that as the fractal dimension of the flocs increases (and the flocs become more compact), the area-to-mass ratio decreases. For most of the observations, certainly for those with $N_f > 2$, this trend appears to be linear. A linear regression of A^* against N_f for all data gives the result:

$$A^* = 0.253 - 0.081N_f \quad (7)$$

($N = 151$, $R^2 = 0.81$, standard errors of intercept and slope 0.008 and 0.003 respectively). For a representative N_f of 2.4, $A^* = 0.06 \text{ m}^2 \text{ g}^{-1}$. A single gram of flocculated particles spread out on a flat surface will fill a square almost $\frac{1}{4}$ metre on a side. For $N_f = 3$,

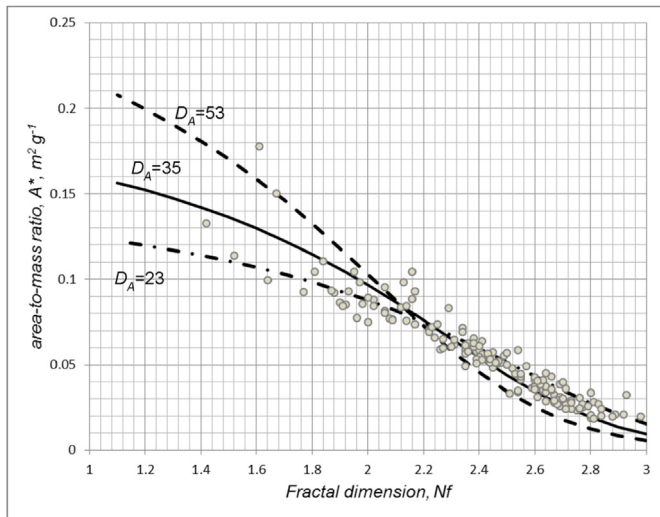


Fig. 5. Observed area-to-mass ratio of particles plotted against their fractal dimension. The model results from Fig. 1b have been superimposed on the observations.

equation (7) gives $A^* = 0.01 \text{ m}^2 \text{ g}^{-1}$ and the equivalent figure for $Nf = 2$ is $0.09 \text{ m}^2 \text{ g}^{-1}$. A change in fractal dimension from 2 to 3 therefore produces a reduction in the area of particles by almost a factor of 10—the factor needed to account for the range of values of mass-specific optical properties.

The fact that the observations in Fig. 5 lie close to the theoretical curves is not surprising; the theory of fractals used to draw the curves has also been used to calculate Nf for the real flocs. What we can learn from this figure is that the *assumptions* in the theory are consistent with observations in the field. First, the Junge formula (equation (3)) is a realistic description of the size distribution over the size ranges measured by the LISST and indeed over the wider size range used for the mass and Nf calculations. This conclusion, as far as the LISST size range is concerned, is supported by the high coefficients of determination obtained when applying equation (3) to the data (Table 1). Secondly, the fractal model gives a realistic way of describing the internal structure of the individual flocs in suspension. The fit of theory to observations does not appear to be hampered greatly by choosing a single fractal dimension to calculate the mass of flocs over a wide range of sizes.

According to the simple theory presented in section 2, the mean size of the flocs should have an influence in a different sense for high and low fractal dimensions. For flocs with fractal dimension less than about 2, A^* is predicted to increase with the mean size of the particles, whereas for Nf greater than 2, A^* should decrease as the particles get larger. To test this prediction, the data were filtered first to select those stations at which $Nf > 2.2$. A multiple regression of A^* on both Nf and Sauter diameter D_A gives the result:

$$A^* = 0.267 - 0.083Nf - 0.000311D_A \quad (8)$$

($N = 115$, $R^2 = 0.64$, standard error of coefficients from left to right 0.016, 0.006 and 0.00009 respectively) from which it can be seen that, for these higher values of the fractal dimension the area-to-mass ratio of the particles decreases with increasing mean floc size in agreement with the theory. For a representative $Nf = 2.4$ (the mean value for our data) equation (8) can be written $A^* = 0.067 - 0.00031D_A$. Sauter diameter varies by an order of magnitude in our data set, from about $10 \mu\text{m}$ to $100 \mu\text{m}$. With these extreme values of D_A , A^* changes from 0.064 to $0.037 \text{ m}^2 \text{ g}^{-1}$. Particle size accounts for a factor of a little less than 2 in the variation of A^*

for this range of sizes.

There is a smaller number of stations for which $Nf < 2$ and here the relationship can be written:

$$A^* = 0.154 - 0.0691Nf + 0.00233D_A \quad (9)$$

($N = 18$, $R^2 = 0.77$, standard error of coefficients from left to right 0.048, 0.021 and 0.0005 respectively). For flocs with low fractal dimension, therefore, the area-to-mass ratio increases with particle size and is more sensitive to particle size than compact high Nf particles, in agreement with the theory (bearing in mind the assumption that area is proportional to D^2 , which may not be appropriate at low fractal dimension). The results shown on Fig. 2 confirm the fact that the main gradient of A^* lies along the fractal dimension axis. Changes in J (or D_A) are less important for A^* , at least for the distribution of observations in our data set.

Finally, we consider the effect of the mineral content of the flocs on their projected area. Mineral material suspended in seawater generally has a higher density than organic material and so we would expect predominantly mineral flocs to be more dense and compact and have a smaller cross sectional area (Hill et al., 2011, 2013). Including the proportion of mineral material in the regression gives the result:

$$A^* = 0.264 - 0.076Nf - 0.0325MSS/TSS \quad (10)$$

($N = 151$, $R^2 = 0.83$, standard error of coefficients from left to right 0.008, 0.003 and 0.008 respectively). The effect of the mineral content of the flocs is statistically significant and in the sense expected. For the mean $Nf = 2.4$, A^* has a value of $0.051 \text{ m}^2 \text{ g}^{-1}$ for flocs which are 100% mineral in content and $0.084 \text{ m}^2 \text{ g}^{-1}$ for flocs which have no mineral content. The change in A^* is close to the factor of 2 expected from the difference in density of mineral and organic material. However, bear in mind that we are extrapolating from the data here. The average mineral content of the flocs in this study is 73% and the range is from 26 to 91% (Table 3). Generally speaking, the flocs in this study are largely mineral in content and typical of those found in shallow energetic shelf seas, rather than in the surface waters of the deep ocean.

4.2. Specific inherent and apparent optical properties and fractal dimension

Each of the 3 optical parameters available in this data set, beam attenuation c , diffuse attenuation K_D and reflection coefficient R generally increase as the mass concentration of particles increases. However, the relationships between the optical coefficients and TSS is somewhat scattered: the ratio of the optical coefficient to mass concentration is not constant. Fig. 6 shows plots of mass-specific attenuation and reflection coefficients against fractal dimension. In each case, the mass-specific optical property decreases as the fractal dimension increases. An important difference between the data in these plots and those shown in the last section is that the optical parameters have been measured *independently* of the LISST observations used to calculate the fractal dimension. These figures provide convincing evidence that the effect of fractal dimension on floc structure influences the passage of light through water in which the flocculated particles are suspended, at least for the type of mineral-dominated floc common in this study.

For the 48 stations in this data set at which measurements of c are available, a regression of beam attenuation against TSS explains 56% of the variance in c . Fig. 6a shows a plot of the mass-specific beam attenuation coefficient ($c^* = c/TSS$) against Nf from which it can be seen that the relationship between these quantities is

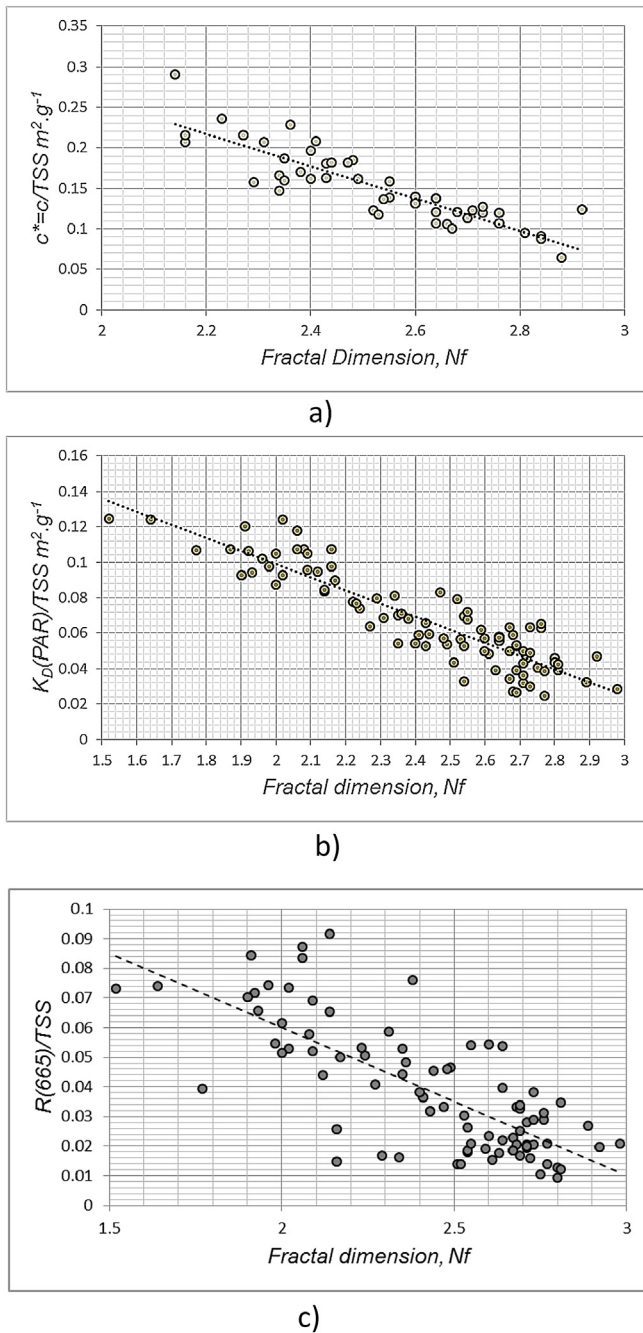


Fig. 6. (a) The mass-specific beam attenuation coefficient at sites 3–8 plotted against the fractal dimension. The dashed line represents a least squares fit to the data and is represented by equation (11) in the text.

(b) The mass-specific diffuse attenuation coefficient for white light plotted against the fractal dimension. The dotted line is a least-squares fit to the data and is represented by equation (12) in the text.

(c) remote sensing, or radiance, reflectance at 665 nm, divided by the total suspended solids concentration and plotted against fractal dimension. The dashed line is a least-squares fit to the points given by equation (13) in the text.

apparently linear and has a negative slope. A linear regression of mass-specific beam attenuation against fractal dimension gives the result:

$$c^* = 0.655 - 0.199N_f \quad (11)$$

($N = 48$, $R^2 = 0.77$, standard error of intercept and slope 0.041 and 0.016 respectively). For the mean fractal dimension for this data set ($N_f = 2.42$) the mass-specific beam attenuation is $0.17 \text{ m}^2 \text{ g}^{-1}$.

The ratio of beam attenuation to particle area is an effective beam attenuation efficiency Q'_C for the particles (Kirk, 2010). For a given mass of flocs, as the fractal dimension changes, the change in beam attenuation will be Q'_C times greater than the change in particle area A . Q'_C can therefore be calculated as the ratio of the slopes in equations (11) and (7), namely $0.199/0.081$, or 2.5. The attenuation efficiency is the sum of scattering efficiency and absorption efficiencies. For particles larger than a few wavelengths of light, the scattering efficiency is about 2.0 and the absorption efficiency is typically an order of magnitude less than this (Bowers et al., 2011) and so a value of 2.5 for the beam attenuation efficiency is reasonable.

The fractal dimension seems to be even more important to the relationship between the diffuse attenuation coefficient and floc concentration. At stations where $K_D(\text{PAR})$ was measured, the suspended particle mass concentration TSS explains just 18% of the variance in $K_D(\text{PAR})$. Dividing $K_D(\text{PAR})$ by TSS to give a mass-specific diffuse attenuation coefficient and regressing this against the fractal dimension gives the result:

$$K_D^* = 0.25 - 0.074N_f \quad (12)$$

($N = 89$, $R^2 = 0.82$, standard error of slope and intercept 0.009 and 0.004 respectively). Bio-physical models of light penetration into the sea, which relate suspended particle concentration to K_D through a constant of proportionality can benefit from this insight that the 'constant' will depend on the fractal dimension of the particles.

Finally, the reflectance in the red part of the spectrum is also sensitive to fractal dimension, although not so clearly as the attenuation coefficients considered above. Fig. 6c shows a plot of $R^* = R(665)/TSS$ (where $R(665)$ is radiance reflectance at 665 nm) against fractal dimension. Particles with a smaller fractal dimension reflect more light, per unit mass, than those with a high fractal dimension. Linear regression of R^* against N_f gives the result:

$$R^* = 0.161 - 0.0502N_f \quad (13)$$

($N = 87$, $R^2 = 0.57$, standard error of intercept and slope 0.011 and 0.005 respectively). Reflection coefficients depend more on backscattering of light than attenuation coefficients and the refractive index of the particles is therefore more important in the case of reflectance. Bowers et al. (2014), for example, showed that the backscattering efficiency depends on the proportion of mineral particles in the total (mineral material having a higher refractive index than organic). Including the ratio MSS/TSS in the regression improves the fit:

$$R^* = 0.102 - 0.0582N_f + 0.0986 \frac{MSS}{TSS} \quad (14)$$

($N = 87$, $R^2 = 0.67$, standard errors of coefficients, from left to right, 0.016, 0.005 and 0.02 respectively). The mineral content of the particles therefore makes a statistically significant contribution to the reflectance of the sea and in a positive sense. The fact that mineral particles are denser and therefore have a smaller area per unit mass can be inferred to be less important than the fact that they have a higher refractive index and are better at backscattering light.

5. Discussion

In the introduction to this paper we presented the case for the importance of the ratio of cross-sectional area and mass of marine particles. This ratio provides the link between optical measurements of particles in suspension in seawater and their mass concentration measured on filters or predicted by theoretical models. For the data set presented in this paper (i.e. mineral-dominated flocs in shelf seas), the area to mass ratio varies by almost an order of magnitude, from 0.02 to 0.18 m² g⁻¹. Much (81% of the variance) of this change can be explained by differences in the way that the flocculated particles are put together, expressed as the fractal dimension. Tightly packed flocs with a fractal dimension close to the maximum value of 3 have the smallest area to mass ratio. More loosely packed flocs with a fractal dimension of 2 have a cross sectional area nearly 10 times greater and, by implication, will have nearly ten times more influence on the passage of light through water. In contrast, changes in both mean particle size and mineral content each affect A^* by a factor less than about 2. The minimal effect of size is consistent with the self-similar fractal nature of the particles, which tend to have the same shape regardless of their size.

These results are consistent with earlier work (Neukermans et al., 2012; Bowers et al., 2009) which showed that the mass specific scattering coefficient of particles depended mostly on their apparent density, with size playing a small role (there is some overlap in the data sets between this and the earlier work, but the present data set is much larger and taken from more sites, albeit with still largely mineral-dominated flocs). Fractal dimension and density are closely related (see appendix): as the fractal dimension of flocs increases the apparent density also increases, approaching the density of the primary particles as N_f nears 3. The relationship between area to mass ratio and apparent density (in kg m⁻³) for this data set can best be expressed:

$$A^* = 0.017 + 20.9 \frac{1}{\rho} \quad (15)$$

($N = 151$, $R^2 = 0.75$, standard error of intercept and slope 0.002 and 0.001 respectively). Apparent density can change by more than an order of magnitude (Table 3 and also see appendix) and the density variation also produces an order of magnitude change in A^* .

A variety of instruments and methods have been used in reaching the conclusions of this work and it is worth noting the inevitable mis-match between some of the observations. The optical measurements of attenuation and reflection coefficients were made over the top 10 m of the water column (or to the bottom in shallow water) as were the LISST measurements. The calculations of particle *area* are therefore based on observations down to this depth. The measurements of particle *mass*, however, are based on samples collected near the sea surface. In shallow water, where the mass concentration increases towards the sea bed, it is likely that a surface measurement of mass underestimates the average mass concentration in the water column. This will affect a small number of stations, however: most measurements were made in a surface mixed layer in deep water.

When calculating fractal dimension by matching theoretical particle mass to observed mass, as we have done in this paper, it is necessary to assume values for the size and apparent density of the primary particles (the smallest particles to which the fractal structure applies). We have taken values of $\rho_0 = 2000$ kg m⁻³ and $D_0 = 4$ μm based on values in the literature. It is possible to derive an overall value of the fractal dimension (which does not require any assumption about primary particles) by plotting apparent density against an estimate of mean particle size (see Fig. 7). The

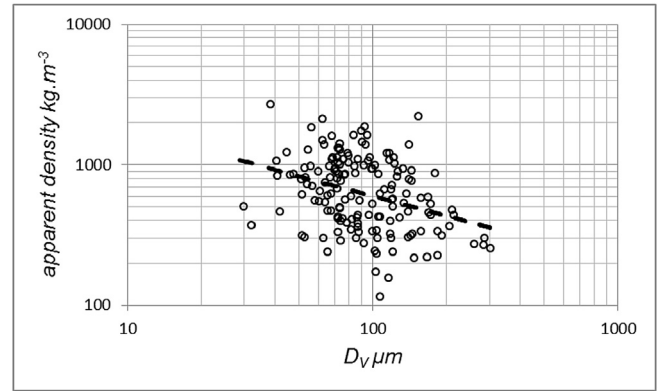


Fig. 7. Apparent density of particles (in units of kg m⁻³) plotted against their median size by volume D_V (μm). The fitted, dashed, line has a slope of -0.47 , which means that the average fractal dimension of the particles in this data set is $N_f = 3 - 0.47$ or 2.53. This value for the mean fractal dimension provides a check on the method used to calculate fractal dimension at each station by matching calculated particle mass to measured mass.

slope of this line, on a log-log plot is equal to $N_f - 3$ (equation (6)). When this procedure is applied to the present data set, using median size by volume on the x-axis, the mean fractal dimension is 2.53 with a standard error of 0.1. This value is consistent with the mean fractal dimension of 2.42 (standard error 0.03) derived by the mass-matching method and supports the choice of primary particle characteristics used in the calculation.

If the fractal dimension is known *a priori*, both the calibration of optical instruments and the prediction of diffuse attenuation in models (and hence light availability for primary production) could be improved using the results of this paper. Unfortunately, theoretical knowledge of the flocculation process is currently too weak to make definitive predictions of N_f for a given set of conditions. It has been suggested that the fractal dimension will increase with the concentration of suspended matter (Kranenburg, 1994). There is some evidence for this in our data. Referring to Fig. 3, the lowest mean value of N_f is observed off the west coast of Scotland, a region of relatively clear water, and the highest values of N_f are observed in areas of fast tidal currents and high turbidity, off Anglesey (site 4) and Burrow Head (site 6). It might be possible to make use of this putative trend. A regression of N_f against TSS for our data set gives:

$$N_f = 2.14 + 0.056TSS \quad (16)$$

($N = 151$, $R^2 = 0.10$, standard error of intercept and slope 0.07 and 0.013 respectively). The relationship between fractal dimension and concentration is therefore weak but statistically significant. This result, although tentative, is consistent with other work. Hill et al. (2011) showed that, for a wide variety of sites, beam attenuation per unit TSS (c^* in our notation) decreases as the maximum reported TSS concentration increased; in agreement with the finding here that c^* decreases as N_f (and therefore TSS) increases. Similarly and again for a wide variety of sites, Bowers and Binding (2006) reported that both mass-specific scattering and beam attenuation coefficients decrease as the water becomes more 'coastal' (and is therefore likely to have a higher suspended particle concentration and also a higher mineral fraction). An immediate application of this work may therefore be to adjust mass-specific optical properties used for deriving suspended load in line with the perceived suspended load. This will require an iterative approach, using an estimate of TSS to refine the specific optical coefficient, leading to a new value of TSS and so on until the estimates converge.

We can use the fractal model to answer a question posed in the introduction: how does the flocculation of particles affect their optical properties? For a fractal particle with representative size D , the cross sectional area will be $A_F = D^2$. If the floc is now broken up into the N primary particles of which it is composed, these will have a cross sectional area of ND_0^2 , D_0 being the size of the primary particles. Using the fractal model, the total area of the individual primaries will be $A_P = (D/D_0)^{Nf} \cdot D_0^2$. The ratio of the area of the floc to that of the individual primary particles is then:

$$\frac{A_F}{A_P} = \left(\frac{D}{D_0}\right)^{2-Nf} \quad (17)$$

If $Nf > 2$, therefore, the area of the floc is less than that of the component particles. The primary particles hide behind each other, reducing the total area and the effect the particle will have on the light field. A floc with a fractal dimension of 2.5, for example, with a size scale 16 times as great as its primary particles will have a cross-sectional area 4 times less than its component parts. As well as increasing the settling speed (and so reducing the suspended matter) flocculation reduces the attenuation of light by the remaining particles. There are thus two ways in which flocculation contributes to clearer seawater.

The main **conclusion** of this paper is that the area to mass ratio of flocculated particles depends primarily on the way that the flocs are constructed. Fractal theory and observations are consistent in showing that the cross-sectional area of a set mass of particles decreases as their fractal dimension increases. A change in fractal dimension from 2 to 3 produces an order of magnitude change in A^* : sufficient, by implication, to explain the observed order of magnitude variation in mass specific beam attenuation and scattering coefficients. Particle size and composition (in terms of mineral content) play a secondary role in controlling the area:mass ratio. Beam and diffuse attenuation coefficients and reflection coefficients used in remote sensing (again expressed per unit mass of particle matter) decrease with increasing fractal dimension. Better calibration of optical instruments for measuring suspended load will result as our understanding of the fractal nature of marine flocs improves. Optical instruments are mostly sensitive to the cross-sectional area of particles but there are other factors that matter, including the refractive index of the particle material. More mineral particles tend to have a higher refractive index and backscattering per unit area tends to increase with mineral content for this reason. However, mineral particles are also more dense and so have a smaller cross-sectional area per unit mass. The overall effect, in this case, is that refractive index is more important than density and remote sensing reflectance per unit concentration tends to increase with the mineral content of the particles. For satellite remote sensing of suspended matter, the opposing effects of refractive index and particle concentration will tend to stabilise the effects of suspended load on reflectance. Moving from deep to coastal water, suspended load will tend to increase (leading to higher fractal dimensions and lower particle area) but mineral content will also tend to increase: so the particles, although of smaller area, will be better at backscattering light.

Acknowledgements

The authors are grateful to the Captain and crew of the R.V. Prince Madog and to the technical support groups at the Universities of Plymouth and Bangor for their invaluable help in gathering these data sets. The work was funded by the UK Natural Environment Research.

Council grants NE/H02090/1 and NE/E014828/1. The paper

benefitted from discussions with Professor Carl Friedrich's group at VIMS in September 2016. The paper has benefitted from suggestions made by 3 anonymous reviewers.

Appendix. The relationship between fractal dimension and density

There are a number of densities that can be associated with a floc. The primary particle density (ρ_0 in our notation) is usually the greatest of these and is always greater than the density of water. The *floc* density can be defined as the total mass of the solids and water in the floc divided by the total volume of the floc. This quantity will also always be greater than the density of water and is the relevant density to use when, for example, calculating the settling speed of the particle. The apparent, or effective density, is the mass of solids (but *not* water) in the floc divided by the total volume of the floc. It can be thought of as the 'dry' mass (as measured on a filter) divided by the 'wet' volume, measured in situ. It is the apparent density that results from measurements of particle mass on a filter and particle volume from in situ optical instruments, such as a camera or LISST. The apparent density, somewhat confusingly, can be less than that of water. It is sometimes assumed that the apparent density is equal to the floc density minus the density of water; Mikkelsen and Pejrup. (2001) show that this is true when the mass of water in the floc is much greater than the mass of solid particles. In this appendix, we explore the relationship between apparent and floc density when the flocs have a fractal structure.

A fractal floc of size D will contain $N=(D/D_0)^{Nf}$ primary particles each of size D_0 and apparent density ρ_0 . The mass of the solids in the floc will therefore be $N \rho_0 D_0^3$ and its total volume (including water) is assumed to be D^3 . The apparent density of the floc (dry mass/'wet' volume) will therefore be:

$$\rho = \frac{N\rho_0 D_0^3}{D^3} = \rho_0 \left(\frac{D}{D_0}\right)^{Nf-3} \quad (A1)$$

for $Nf = 3$, the apparent density is therefore equal to component particle density, as we would expect for compact flocs with no space between the component particles. As Nf tends to 1 (and for $D \gg D_0$) the apparent density tends to zero; the apparent density can certainly become much less than the density of water if it is the case that particle volume scales as D^3 . Fig. A1 shows the variation of apparent density with fractal dimension assuming $\rho_0 = 2000 \text{ kg m}^{-3}$, $D_0 = 4 \text{ }\mu\text{m}$ and for a representative $D = 20 \text{ }\mu\text{m}$.

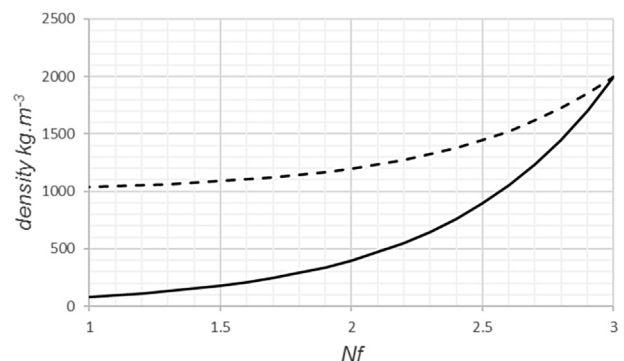


Fig. A1. Variation of apparent density (continuous curve) and floc density (dashed curve) with fractal dimension, Nf . As the fractal dimension approaches 1, the difference between these two measures of density approaches the density of water.

The floc density, the mass of solids plus water in the floc, divided by the floc volume can be written:

$$\rho_F = \frac{N\rho_0 D_0^3 + (D^3 - ND_0^3)\rho_W}{D^3}$$

where $(D^3 - ND_0^3)$ is the volume of water in the floc and ρ_W is the density of water. Rearranging and substituting $N=(D/D_0)^{Nf}$ gives.

$$\rho_F = \rho_W + (\rho_0 - \rho_W)\left(\frac{D}{D_0}\right)^{Nf-3}$$

for compact flocs with $Nf = 3$, floc density is therefore equal to the density of the component particles as we would expect. As the fractal dimension approaches 1 (and for $D \gg D_0$) floc density

approaches the density of water (Fig. A1). The difference between floc density and apparent, or effective density is therefore.

$$\rho_F - \rho = \rho_W \left(1 - \left(\frac{D}{D_0}\right)^{Nf-3}\right)$$

from which it can be seen that for compact flocs with $Nf = 3$, the difference between floc and apparent density tends to zero. For $Nf = 1$ (and $D \gg D_0$) the floc density is equal to the apparent density plus the density of water.

Table 1
Notation.

Symbol	Meaning	units
<i>A</i>	Cross-sectional area of particles in suspension	m ²
<i>A_F, A_P</i>	Cross sectional area of flocs and primary particles, respectively	m ²
<i>A*</i>	Area-to-mass ratio of particles <i>A</i> /TSS	m ² g ⁻¹
<i>c</i>	Beam attenuation coefficient	m ⁻¹
<i>c*</i>	Mass-specific beam attenuation <i>c</i> /TSS	m ² g ⁻¹
<i>D</i>	Particle size	μm
<i>D₀</i>	Primary particle size	μm
<i>D_A</i>	Sauter diameter <i>V</i> / <i>A</i>	μm
<i>D_V</i>	Median size by volume	μm
<i>J</i>	Slope of the particle size distribution	
<i>K_D(PAR)</i>	Diffuse attenuation coefficient for white light	m ⁻¹
<i>K*</i>	Mass-specific diffuse attenuation for PAR <i>K_D(PAR)</i> /TSS	m ² g ⁻¹
<i>M</i>	Mass of solid material per unit volume of water (used in theoretical calculations)	g m ⁻³
<i>MSS</i>	Mineral suspended sediments concentration	g m ⁻³
<i>N</i>	Number of primary particles in a floc. Also used for number of observations or stations	
<i>Nf</i>	Fractal dimension	
<i>n</i>	Number of flocs in suspension	
<i>Q_c</i>	Effective beam attenuation efficiency <i>c</i> / <i>A</i>	
<i>R(665)</i>	Remote sensing reflectance at 665 nm	Sr ⁻¹
<i>R*</i>	Mass-specific reflectance <i>R(665)</i> /TSS	
<i>TSS</i>	Total suspended sediments concentration	g m ⁻³
<i>V</i>	Total volume of particles in suspension	
<i>ρ</i>	Particle apparent density TSS/ <i>V</i>	Kg m ⁻³
<i>ρ₀</i>	Primary particle apparent density	Kg m ⁻³
<i>ρ_F, ρ_W</i>	Floc density and water density, respectively	Kg m ⁻³

Table 2

Summary of results from different campaigns. *N* is the number of stations, TSS the total suspended solids, MSS/TSS the ratio of mineral to total solids, *V* the total volume of suspended matter measured by the LISST, *ρ* the apparent density of the flocs, *J* the estimated slope and *R*² the coefficient of determination from fitting the Junge distribution to the data. *Nf* is the fractal dimension, *D_A* the particle size by area and *A** the area/mass ratio of the particle suspension. Location numbers refer to sites and dates as follows: 1, Plymouth Sound, 17/6/08; 2 Tamar estuary, 19/6/08; 3 North Anglesey, 20/4/09; 4 West Anglesey, 20–21/4/09; 5 Isle of Man, 23/4/09; 6 Burrow Head, 19/7/09; 7 Solway Firth, 20/7/09; 8 Conwy Bay, 21/7/09; 9 Menai Strait spring tides, 17/8/11; 10 Menai Strait neap tides, 23/8/11; 11 West Scotland, 15–22/6/12.

Location	<i>N</i>	TSS mg l ⁻¹	MSS/TSS	<i>V</i> μl ⁻¹	<i>ρ</i> kg m ⁻³	<i>J</i>	<i>R</i> ²	<i>Nf</i>	<i>D_A</i> μm	<i>A*</i> m ² g ⁻¹
1	24	5.14	0.80	6.21	994	3.52	0.98	2.70	39.3	0.033
2	30	5.21	0.75	12.70	445	3.60	0.99	2.04	31.5	0.080
3	5	4.12	0.64	12.68	349	3.41	0.97	2.29	27.4	0.079
4	24	4.33	0.79	4.48	1114	3.66	0.99	2.65	27.4	0.038
5	4	5.78	0.74	14.40	674	3.51	0.99	2.50	44.9	0.053
6	9	4.12	0.86	4.11	1087	3.47	1.00	2.72	39.2	0.026
7	6	5.92	0.82	9.84	662	3.55	1.00	2.49	31.9	0.052
8	13	7.12	0.82	15.24	510	3.47	1.00	2.38	38.8	0.057
9	13	6.57	0.68	12.66	611	3.65	1.00	2.45	27.7	0.070
10	15	5.84	0.70	5.85	1016	3.73	1.00	2.53	23.0	0.045
11	15	2.16	0.39	8.40	265	3.50	0.99	1.90	37.4	0.115

Table 3
Statistics for all data (N = 151).

	Mean	Median	Minimum	maximum	Standard deviation
TSS mg l ⁻¹	5.06	4.94	0.91	15.40	1.83
MSS/TSS	0.73	0.77	0.26	0.91	0.14
V μl l ⁻¹	8.85	7.18	1.69	30.63	5.45
ρ kg m ⁻³	741	623	116	2134	408
J	3.57	3.59	3.17	3.89	0.13
R ² for J fit	0.99	0.99	0.90	1.00	0.01
Nf	2.42	2.45	1.42	2.98	0.32
D _A μm	33.3	30.92	14.5	117.9	11.0
A* m ² g ⁻¹	0.056	0.056	0.019	0.178	0.029

References

- Agrawal, Y.C., Pottsmith, H.C., 2000. Instruments for particle size and settling velocity observations in sediment transport. *Mar. Geol.* 168, 89–114.
- Babin, M., Morel, A., Fournier-Sicre, V., Fell, F., Stramski, D., 2003. Light scattering properties of marine particles in coastal and open ocean waters as related to the particle mass concentration. *Limnol. Oceanogr.* 48, 843–859.
- Baker, E.T., Lavelle, J.W., 1984. The effect of particle size on the light attenuation coefficient of natural suspensions. *J. Geophys. Res.* 89, 8197–8203.
- Bale, A.J., Tocher, M.D., Weaver, R., Hudson, S.J., Aiken, J., 1994. Laboratory measurements of spectral properties of estuarine suspended sediments. *Neth. J. Aquatic Ecol.* 28, 237–244.
- Binding, C.E., Bowers, D.G., Mitchelson-Jacob, E.G., 2005. Estimating suspended sediment concentrations from ocean colour measurements in moderately turbid water; the impact of variable particle scattering properties. *Remote Sens. Environ.* 94, 373–383.
- Bowers, D.G., Binding, C.E., 2006. Optical properties of mineral suspended particles in the sea: a review and synthesis. *Estuar. Coast. Shelf Sci.* 67, 219–230.
- Bowers, D.G., Braithwaite, K.M., Nimmo-Smith, W.A.M., Graham, G.W., 2009. Light scattering by particles suspended in the sea: the role of particle size and density. *Cont. Shelf Res.* 29, 1748–1755.
- Bowers, D.G., Braithwaite, K.M., Nimmo-Smith, W.A.M., Graham, G.W., 2011. Optical efficiency of flocs in shelf seas and estuaries. *Estuar. Coast. Shelf Sci.* 91, 341–350.
- Bowers, D.G., Braithwaite, K.M., 2012. Evidence that satellites sense the cross-sectional area of suspended particles in shelf seas and estuaries better than their mass. *Geo-Marine Lett.* 32, 165–171.
- Bowers, D.G., Hill, P.S., Braithwaite, K.M., 2014. The effect of particulate organic content on the remote sensing of marine suspended sediments. *Remote Sens. Environ.* 144, 172–178.
- Braithwaite, K.M., Bowers, D.G., Nimmo-Smith, W.A.M., Graham, G.W., Agrawal, Y.C., Mikkelsen, O.A., 2010. Observations of particle density and scattering in the tamar estuary. *Mar. Geol.* 277, 1–10.
- Chen, S., Eisma, D., 1995. Fractal geometry of in situ flocs in the estuarine and coastal environment. *Neth. J. Sea Res.* 33, 173–182.
- Dyer, K.R., Manning, A.J., 1995. Observations of the size, settling velocity and effective density of flocs and their fractal dimensions. *J. Sea Res.* 41, 87–95.
- Eisma, D., Schhmacher, T., Boekel, H., Van Heerwaarden, J., Franken, H., Laan, M., Vaars, A., Eijgenraam, F., Kalf, J., 1990. A camera and image analysis system for in situ observations of flocs in coastal waters. *Neth. J. Sea Res.* 27, 43–56.
- Fettweis, M., 2008. Uncertainty of excess density and settling velocity of mud flocs derived from in situ measurements. *Estuar. Coast. Shelf Sci.* 78, 426–436.
- Gohin, F., Loyer, S., Lunven, M., Labry, C., Froidefond, J.M., Delmas, D., Huret, M., Herbland, A., 2005. Satellite-derived parameters for biological modelling in coastal waters: illustration over the eastern continental shelf of the Bay of Biscay. *Remote Sens. Environ.* 95, 29–46.
- Graham, G.W., Davies, E.J., Nimmo-Smith, W.A.M., Bowers, D.G., Braithwaite, K.M., 2012. Interpreting LISST 100X measurements of particles with complex shape using in-line holography. *J. Geophys. Res.* 117, C05034.
- Guillou, N., Rivier, A., Gohin, F., Chapalain, G., 2015. Modelling near-surface suspended sediment concentrations in the english channel. *J. Mar. Sci. Eng.* 3, 193–215.
- Hill, P.S., Syvitski, J.P., Cowan, E.A., Powell, R.D., 1998. In situ observations of floc settling velocities in Glacier Bay, Alaska. *Mar. Geol.* 145, 85–94.
- Hill, P.S., Boss, E., Newgard, J.P., Law, B.A., Milligan, T.G., 2011. Observations of the sensitivity of beam attenuation to particle size in a coastal bottom boundary layer. *J. Geophys. Res. (Oceans)*. <http://dx.doi.org/10.1029/2010JC006539>.
- Hill, P.S., Bowers, D.G., Braithwaite, K.M., 2013. The effect of suspended particle composition on particle area-to-mass ratios in coastal waters. *Methods Oceanogr.* 7, 95–109.
- Jones, S.E., Jago, C.F., Simpson, J.H., 1996. Modelling suspended sediment dynamics in tidally stirred and periodically stratified waters: progress and pitfalls. In: *Mixing in Estuaries and Coastal Seas; Coastal and Estuarine Studies*, vol 50. American Geophysical Union, pp. 302–303.
- Khelifa, A., Hill, P.S., 2006. Models for effective density and settling speed of flocs. *J. Hydraulics Res.* 44, 390–401.
- Kilps, J.E., Logan, B.E., Alldredge, A.L., 1993. Fractal dimensions of marine snow determined from image analysis of in situ photographs. *Deep Sea Res.* 41, 1159–1169.
- Kirk, J.T.O., 2010. *Light and Photosynthesis in Aquatic Ecosystems*, third ed. Cambridge University Press.
- Kranenburg, C., 1994. The fractal structure of cohesive sediment aggregates. *Estuar. Coast. Shelf Sci.* 39, 451–560.
- Krone, R.B., 1963. *Flume Studies of the Transport of Sediment in Estuarial Shoaling Processes*. Report. Hydraulic Engineering Laboratory and Sanitary Engineering Laboratory, University of California, Berkeley.
- Markussen, T.N., Elberling, B., Winter, C., Andersen, T.J., 2016. Flocculation of meltwater particles control Arctic land-sea fluxes of labile iron. *Nat. Sci. Rep.* 6 <http://dx.doi.org/10.1038/srep24033>.
- Mikkelsen, O.A., Pejrup, M.J., 2001. The use of a LISST-100 laser particle sizer for in situ estimates of floc size, density and settling velocity. *Geo-Marine Lett.* 20, 187–195.
- Mitchell, C., Cunningham, A., McKee, D., 2014. Remote sensing of shelf sea optical properties: evaluation of a quasi-analytical approach for the Irish sea. *Remote Sens. Environ.* 143, 142–153.
- Neukermans, G., Loisel, H., Meriaux, X., Astoreca, R., McKee, D., 2012. In situ variability of mass-specific beam attenuation and backscattering of marine particles with respect to particle size, density and composition. *Limnol. Oceanogr.* 57, 124–144.
- Schulz, R., Hichenbach, M., Langevin, Y., 22 others, 2015. Comet 67P/Churyumov-Gerasimeko sheds dust accumulated over the past 4 years. *Nature* 518, 216–218.
- Stavn, R.H., 2011. Mass-specific scattering cross-sections of suspended sediments and aggregates: theoretical limits and applications. *Opt. Express* 20, 201–219.
- Stein, T.H.M., Westbrook, C.D., Nicoll, J.C., 2015. Fractal geometry of aggregate snowflakes revealed by triple-wavelength radar measurements. *Geophys. Res. Lett.* <http://dx.doi.org/10.1002/2014GL062170>.
- Winterwerp, J.C., 1998. A simple model for turbulence induced flocculation of cohesive sediment. *J. Hydraulic Res.* 36, 309–326.